Int J Adv Manuf Technol (2018) 94:175–189
DOI 10.1007/s00170-017-0801-4

ORIGINAL ARTICLE

# Analytical approach of asymmetrical thermomechanical rolling by slab method

**N. A. Razani**[1] · **B. Mollaei Dariani**[1] · **M. Soltanpour**[2]

Received: 11 May 2017 / Accepted: 11 July 2017 / Published online: 9 August 2017
© Springer-Verlag London Ltd. 2017

**Abstract** In this paper, based on the slab method and focusing on the rate-dependent flow condition, asymmetrical thermomechanical rolling (ATMR) is investigated to establish a new model for calculation of the rolling force. Unlike the former models where the rate-dependent condition of the yield shear stress has not been considered, in this study, a visco-plastic flow stress formulation of material is used for applying the rate and temperature sensitivity parameters and kinetic of work hardening and softening of the material. Comparison of the present analytical model with experimental data and other models reveals the precision of calculation. An asymmetrical rolling index (ARI) is introduced to evaluate the effects of rolling parameters on asymmetrical conditions of the rolling process. Using the response surface methodology (RSM), the interaction effects and contribution of rolling parameters are studied. Investigations indicate that the speed rate plays a role as an intensifier of the parameters' effect on the ARI. Furthermore, the occurrence of high value of speed rate with a low percent of thickness reduction leads to the restricted rise of the ARI levels. The verification of the statistical models indicates an acceptable competency of results.

**Keywords** Asymmetrical thermomechanical rolling (ATMR) · Slab method · Asymmetrical rolling index (ARI) · Response surface methodology (RSM)

✉ B. Mollaei Dariani
dariani@aut.ac.ir

[1] Mechanical Engineering Department, Amirkabir University of Technology, 424 Hafez Ave, Tehran 15875-4413, Iran

[2] Faculty of Engineering and Technology, Imam Khomeini International University, Persian Gulf Ave, District 3, Qazvin 3414916818, Iran

## 1 Introduction

Based on various models, there are different studies performed in the analytical field of rolling forces. Because of the significance rule of the rolling force on rate of power consuming, rolling stand vibration, and equipment's lifetime, the quantity of established works is very widespread. Researchers have presented several analytical models with varying hypotheses in rolling stress investigation approach. Recently, analysis of asymmetrical rolling has been used for evaluation of the slab outgoing curvature from stand roll gap and rolling force [1]. Because of the friction condition in the rolling process, especially in the thermomechanical rolling (TMR), variation in the interface condition of the slab and the rolls, different roll diameters, rolls' speed mismatch, different temperatures in the upper and lower surface of the slab in rolling region and horizontal and vertical deviations of the roll axis from pass-line and the slab caused varying distribution strain and strain rates and different distribution stresses imposing in the deformed region, consequently. This unequal distribution of deformation parameters leads to asymmetrical deformation during the TMR process. In the asymmetrical rolling, in addition to the inlet and outlet zones in the roll gap, there is a third zone named cross shear region (CSR) inclosing between neutral points. In this region, the upper and the lower friction shear stresses are imposed in opposite directions. For performing an accurate calculation of rolling force, analysis of asymmetrical rolling is very efficient, as some researchers have revealed that the amount of predicted rolling force in the asymmetrical analysis is less than the symmetrical analysis [2, 3]. In the rolling industry, effective rolling parameters are changed into a route to create asymmetrical rolling conditions, naturally, though sometimes the asymmetrical conditions are imposed to the rolling stand by operators. For example, in order to control the sheet curvature index in the roll gap exit, by setting the

speed mismatch of rolls, a feature named ski is created to keep from hitting the head of sheet and the run out table.

In the literature, the rigidity behavior, plane strain plastic deformation, and Von Mises yield criterion have been mostly assumed.

Hwang et al. [4–6] have presented the first advanced studies in the analysis of asymmetrical rolling based on the slab method. Due to various procedures, they have studied alternatively the rolling force by applying Von Mises and Tresca criteria, shearing compression slip line theory, imposing shear stress and internal moment, and constant and variant sticking friction condition.

Tzou [7], establishing a relation between friction coefficient and friction factor, has evaluated the influences of roll speed rate, thickness reduction percentage, and tension (forward and backward) in asymmetrical rolling. Salimi and Sasani [8] have carried out an analysis like Hwang's one with different friction condition. They have neglected of bit angle effect. Kadkhodaei et al. [2] have attempted to investigate the effect of vertical deviation of the lower roll from the slab in the input section of the roll gap by an analytical model in a sticking friction condition. For considering the asymmetrical rolling based on Salimi's model in slipping-sticking friction conditions, Mousavi et al. [9] have executed the effects of speed mismatch of the rolls on the distribution of the normal and shear stresses and compared with FEM results. Based on Salimi's model, Gudur et al. [10] have made a new attempt including the work hardening in flow stress function of the rolled material and friction model of Wenheim and Bay. Their model presented a good agreement result comprising experimental works. Tian et al. [11], assuming the constancy of friction along the length of contact surfaces and neglecting the shear stress in vertical surfaces of internal sides of the CSR, have demonstrated that with increasing the speed rate of the rolls, the length of the CSR would be extended.

Assuming a second-order function of shear stress and a linear function imposed normal stress on the vertical side of the slab, Qwamizadeh et al. [3] have attempted to detect the neutral point position and curvature index of the sheet. Same as Tian's model and by imposing the shear stresses on the vertical sides of triplet regions of the deformed cross section, Zhang et al. [12] have analyzed the asymmetrical rolling in sticking friction conditions. In comparison, Zhang worked with Salimi's model, Hwang's model, and experimental results; Salimi's model has presented more accurate results than other models. Assuming the slipping friction conditions in the entrance and exit of the roll gap and sticking friction conditions in the CSR of the roll gap, Chen et al. [13] have studied the stress distribution along the length of contact interface and the effects of friction conditions, flow stress, and roll distortion. Imposing the non-uniform normal and shear stress in the asymmetrical rolling of two-layer sheet, Qwamizadeh et al. [14] and Afrouz and Parvizi [15] have evaluated the rolling force, outgoing curvature, and neural point position in the roll gap. Concentrating on the CSR, Tang et al. [16] have presented a relationship between cross-shear ratio and exit thickness reduction. They developed a new formulation to predict the minimum permissible foil thickness in the asymmetrical rolling. Aboutorabi et al. [1] have proposed a model based on Salimi's model by inserting horizontal deviation axis of the upper rolling roll from lower one. They have presented a fourth region near the entrance of the roll gap and have calculated the curvature of the slab in the entrance and exit of the roll gap.

In spite of expanded procedure of usage of the finite element method in 2D and 3D modeling of the asymmetrical rolling, simplification and reduction of time-consuming calculations in analytical methods are the evident competition advantages. In the asymmetrical rolling process, especially TMR, yield shear stress has been influenced by conditions of unequal distribution of strain, strain rate, temperature, and microstructure. However, in the accomplished analytical model of the slab method approach, in spite of the variety of strain and strain rate, the yield shear stress has been assumed as a constant value.

In TMR process, the presence of features, including work hardening (WH), dynamic recovery (DRV), dynamic recrystallization (DRX), and variety of grain size (GS) during deformation, leads to an unstable condition for flow curve of material [17]. In addition, the difference of strain, strain rate, and temperature in the upper and lower contact surface and the unequal diameter of the rolls intensify the unsteadiness of the material flow. Comprising the symmetrical and the asymmetrical hot rolling of steel, Liu and Kawalla [18] have indicated that the high diameter ratio of rollers leads to the high value of grain refinement. By evaluating the aluminum texture, Wronski et al. [19] have found that the asymmetrical rolling improves the microstructure and the homogeneity of material texture. Performing a comprehensive study of the advanced rolling techniques by Yu et al. [20] revealed that the asymmetrical rolling can improve the final mechanical property of rolled material.

In this study, the purpose was to develop the analysis of the asymmetrical thermomechanical rolling (ATMR) by imposing the rate-dependent yield shear stress due to the dynamic condition of unsteady strain, strain rate, and work hardening and softening. Hence, in the present model, diversity between yield shear stress in the upper and lower interfaces of the roll gap confining between the slab and the rolls is assumed. These rate-dependent conditions are performed for the first time in the analytical model.

Furthermore, because of the inequality of the rolls' radii, the initial slab thickness in the upper and lower portion of the slab is assumed to be unequal. Hence, in this study, a novel analytical model is introduced based on a new description of the deformation region in the roll gap. Concentrating on the

CSR morphology, an asymmetrical rolling index (ARI) is introduced to evaluate the effects of the rolling parameters on asymmetrical conditions. After verification of the model output by experimental date for pipeline API-5L X70 microalloy steel and pressure vessel steel of P265GH, using response surface method (RSM) as an applicable tool of DOE, the interaction effects and contribution of parameters on the ARI and rolling force are investigated.

## 2 Asymmetrical rolling mathematical model analysis

Regarding Fig. 1, ATMR is developed based on the slab method using the following assumptions:

1. Plain strain plastic deformation.
2. Horizontal direction of the slab in entrance and exit of the roll gap neglecting of bit angle effect.
3. Linear differential of normal stress distribution in element's sides.
4. Constancy of temperature distribution in the upper and lower surfaces of the roll gap.
5. Regarding unequal rolls' radii, the thickness of the slab is supposed to be intersect from the $x$-axis.
6. Sticking friction conditions of the slab and the rolls' interfaces ($m_u$, $m_l$).
7. Friction shear stress is variable corresponding to yield shear stress, strain, and strain rate distribution ($\tau_{u,l} = m_{u,l} k_{u,l}$).
8. In comparison with the roll circumference, the rolls' contact length is assumed to be very small using the following relationship [21]

$$L = \frac{\{(h_i - h_0)(2R_u + h_0 - h_i)(2R_l + h_0 - h_i)[2(R_u + R_l) + (h_0 - h_i)]\}^{1/2}}{2(R_u + R_l + h_0 - h_i)} \quad (1)$$

Regarding the stress field of the cross section that has been positioned at $x$ distance from the exit of the roll gap, the following equations can be extracted [3]

$$h_u = \frac{h_0}{2} + R_u - \sqrt{R_u^2 - x^2} \quad (2)$$

$$h_l = \frac{h_0}{2} + R_l - \sqrt{R_l^2 - x^2} \quad (3)$$

$$h = h_u + h_l = h_0 + R_u + R_l - \left(\sqrt{R_u^2 - x^2} + \sqrt{R_l^2 - x^2}\right) \quad (4)$$

Referring to Fig. 2, in the first portion of the deformed region, the roll speed is more than the slab speed. So, the directions of friction force in the upper and lower interfaces are in forward direction. In the third portion of the deformed region, the condition is reversed as the slab speed is more than the rolls' speed. Hence, in this portion, the direction of imposing friction forces on the interfaces is in the opposite direction

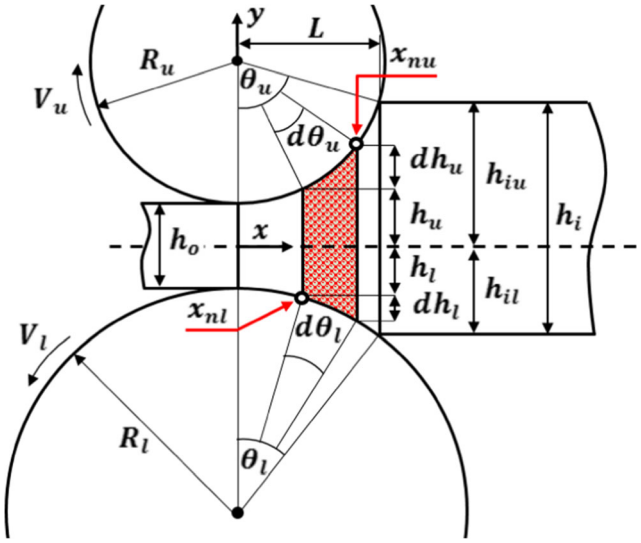


**Fig. 1** Asymmetrical roll gap geometry

of the rolling process. Assuming that the circumferential speed of the lower roll is more than that of the upper roll, the location of the lower neutral point is nearer to the rolling exit. Therefore, in the second portion of the deformed region, the flow speed of the lower surface of the slab is more than that of the slab upper surface. This speed mismatch of the slab and the rolls leads to unlike direction of friction force in the upper and lower interface.

According to the interaction resultant of imposing normal and shear stress and moment on the point O of the first portion, indicated in Fig. 2, equilibrium equations are given by the following relation [10]

$$\sum F_x = 0 \Rightarrow \left(\frac{p_u}{R_u} + \frac{p_l}{R_l}\right)x - \frac{x}{R_{eq}}(\sigma_u + \sigma_l) - (\tau_u + \tau_l) - \frac{h}{2}\left(\frac{d\sigma_u}{dx} + \frac{d\sigma_l}{dx}\right) = 0 \quad (5)$$

$$\sum F_y = 0 \Rightarrow \frac{2x}{R_{eq}}\tau + (p_l - p_u) + \left(\frac{\tau_l}{R_l} - \frac{\tau_u}{R_u}\right)x + h\frac{d\tau}{dx} = 0 \quad (6)$$

$$\sum M_{O^*} = 0 \Rightarrow \tau h + \frac{xh}{2}\left(\frac{p_l}{R_l} - \frac{p_u}{R_u}\right) + \frac{xh(\sigma_u + \sigma_l)}{2R_u} + \frac{h}{2}(\tau_u - \tau_l) - \frac{xh(\sigma_u + 5\sigma_l)}{6R_{eq}} + \frac{h^2}{12}\left(\frac{d\sigma_u}{dx} - \frac{d\sigma_l}{dx}\right) = 0 \quad (7)$$

As illustrated in Fig. 2, unlike zone I, the directions of the upper and lower friction stress in zone III are both forward. Because, unlike zone I, the velocities of the upper and lower rolls are both higher than that of the slab. The asymmetry of rolling leads to the movement of the position of the upper and lower neutral points in opposite direction and creates a new middle zone II. In this zone, the velocity of the upper roll is lower than that of the slab and the velocity of the lower roll is higher than that of the slab. So, the directions of the upper and lower friction stress in zone II are not the same. By sorting the

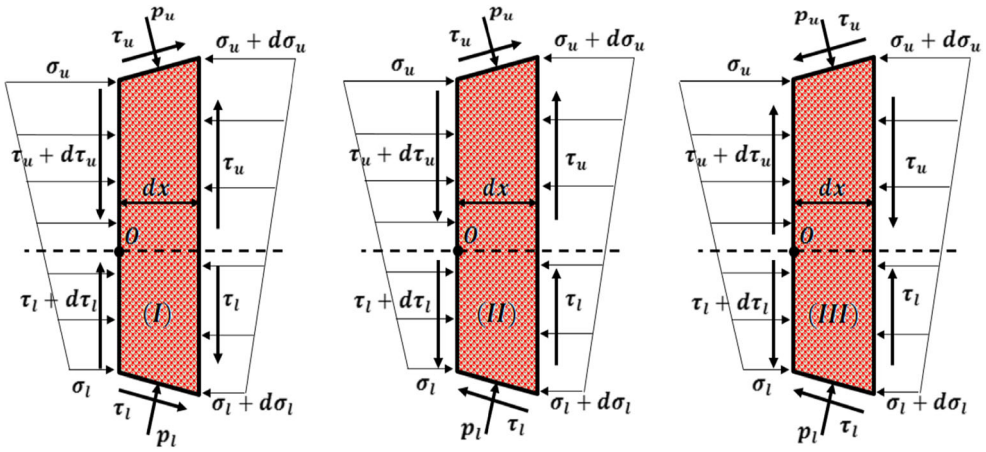


**Fig. 2** Equilibrium diagram and stress field of elements in deformed triple regions

differential terms of normal stresses toward $x$ direction in Eqs. (5) and (7), the set of following equations can be obtained:

$$A = \left(\frac{d\sigma_u}{dx} + \frac{d\sigma_l}{dx}\right) = \frac{2x}{h}\left(\frac{p_u}{R_u} + \frac{p_l}{R_l}\right) - \frac{2x}{hR_{eq}}(\sigma_u + \sigma_l) - \frac{2}{h}(\tau_u + \tau_l) \tag{8}$$

$$B = \left(\frac{d\sigma_l}{dx} - \frac{d\sigma_u}{dx}\right) = \frac{12}{h}\tau + \frac{6x}{h}\left(\frac{p_l}{R_l} - \frac{p_u}{hR_u}\right) + \frac{6x}{hR_u}(\sigma_u + \sigma_l) + \frac{6}{h}(\tau_u - \tau_l) - \frac{2x}{hR_{eq}}(\sigma_u + 5\sigma_l) \tag{9}$$

## 3 Friction condition

Assuming the sticking friction conditions in the interfaces between the slab and the rolls, the imposed shear friction stresses on the upper and lower surfaces of the roll gap are presented as the following equations

$$\tau_u = m_u k_u \quad , \quad \tau_l = m_l k_l \tag{10}$$

Because of the unequal distribution of speed mismatching of the rolls and the resulting strain rate variety in the upper and lower interfaces, the yield shear stresses of $k_u$ and $k_l$ are identified to represent asymmetrical material flow in the roll gap. This distinguishing of material flow in the upper and lower surfaces of the roll gap is performed for the first time in the analytical model.

Referring to Fig. 3, this asymmetrical material flow leads to unequal yield shear stress and friction stress distribution in the deformed region in the roll gap. Because of work hardening and softening features, the curves of shear stress imposing on the vertical side of thickness elements (vertical axis $y$: vertical distance from the centerline of the slab) are different. So, the asymmetrical condition of the upper and lower surface of the deformed region leads to non-uniformity of material flow in the upper and lower surfaces.

## 4 Yield criterion

Plastic flow rule of Levy–Mises in plane strain condition is used based on the following relationships

$$\tau_{xz} = \tau_{yz} = 0 \quad , \quad \sigma_z = \frac{\sigma_x + \sigma_y}{2} \tag{11}$$

Therefore, aimed to Von Mises yield criterion, the flow rule for each element of the upper and lower surfaces can be given by [21]

$$\left|\frac{\sigma_x + \sigma_y}{2}\right| = \sqrt{k^2 - \tau_{xy}^2} \quad , \quad k = \overline{\sigma}/\sqrt{3} \tag{12}$$

So, assuming the small bit angle, the normal stress in upper and lower can be derived as follows

$$\sigma_u = p_u - 2k_u\sqrt{1 - m_u^2} \tag{13}$$

$$\sigma_l = p_l - 2k_l\sqrt{1 - m_l^2} \tag{14}$$

## 5 Visco-plastic flow stress

In order to include rate-dependent, work hardening, and work softening feature in the material flow stress, the visco-plastic model of Yanagida et al. [22] is used for flow stress acquisition as the following equations

$$\begin{cases} \sigma_{u,l} = F_1 \bar{\varepsilon}_{u,l}^{\,n} \dot{\bar{\varepsilon}}_{u,l}^{\,m} \exp\left[C\left(\frac{1}{T_{u,l}} - \frac{1}{T_0}\right)\right] & \left(\bar{\varepsilon} \le \varepsilon_c\right) \\ \sigma_{u,l} = \left(F_2 \exp\left[a\left(\bar{\varepsilon}_{u,l} - \bar{\varepsilon}_{\max}\right)^2\right] + F_3\right) \dot{\bar{\varepsilon}}_{u,l}^{\,m} \exp\left[C\left(\frac{1}{T_{u,l}} - \frac{1}{T_0}\right)\right] & \left(\bar{\varepsilon} > \varepsilon_c\right) \end{cases} \tag{15}$$

where $n$ is the strain hardening parameter, $m$ is the strain rate-dependent term, and $C$ is the temperature-dependent term. The term $\varepsilon_c$ is the critical strain to define the onset of DRX and $\varepsilon_{max}$ is the relative strain at maximum stress of the flow curve.

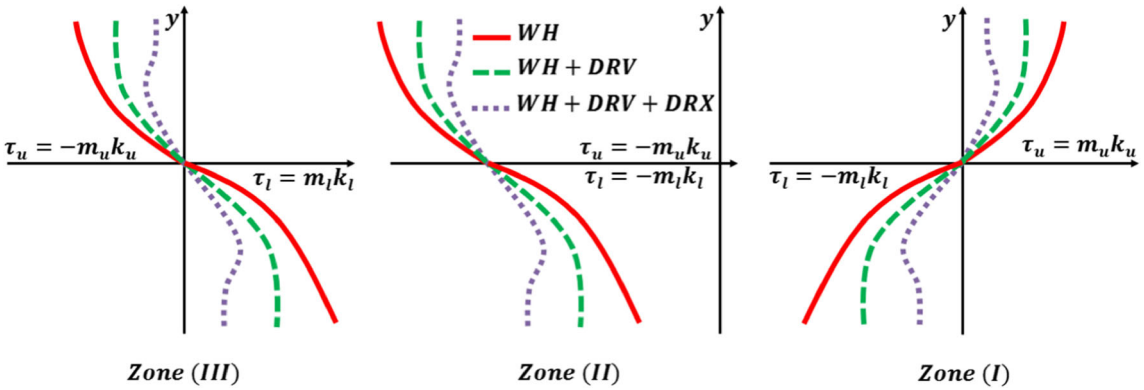


**Fig. 3** Unequal distribution of shear stress in triple regions in the roll gap

The terms $F_1$ , $n$ , $F_3$ and $\varepsilon_c$ are defined as independent parameters calculated in inverse analysis of hot compression test, and the terms $a$ and $F_2$ are the functions of the mentioned independents' parameters. The parameters $T$ and $T_0$ are the temperature of the roll gap and reference temperature, respectively [22].

Where $\bar{\varepsilon}$ and $\dot{\bar{\varepsilon}}$ are the effective strain and strain rates, respectively. In plane strain condition, these components are given by the following formulation [23, 24]:

$$\bar{\varepsilon}_{u,l} = \frac{2}{\sqrt{3}} \ln \frac{h_{iu,il}}{h_{u,l}} \quad , \quad \dot{\bar{\varepsilon}}_{u,l} = \frac{2}{\sqrt{3}} \frac{V_{u,l}}{L} \ln \frac{h_{ih,il}}{h_{u,l}} \tag{16}$$

$$h_{iu} = \frac{h_0}{2} + R_u - \sqrt{{R_u}^2 - L^2} \quad , \quad h_{il} = \frac{h_0}{2} + R_l - \sqrt{{R_l}^2 - L^2} \tag{17}$$

In which $V$ is the circumferential speed of the roll and $h_{iu}$, $h_{il}$, $h_u$, and $h_l$ are the upper and lower slab thicknesses in entrance and exit of the roll gap, respectively. Because the variation of the horizontal character of $x$ leads to diversity in thickness and rate-dependent conditions, the rate-dependent flow stress of the rolled material can be presented as a function of $x$. So by differentiating constitution equation of flow stress (Eq. (15)) with respect to $x$

$$\frac{d\sigma}{dx} = Q \frac{dh}{dx} \Rightarrow \frac{dk}{dx} = \frac{Q}{\sqrt{3}} \frac{dh}{dx} \tag{18}$$

where $Q$ is named differential stress factor. Differentiating of $\bar{\varepsilon}$ and $\dot{\bar{\varepsilon}}$ is with respect to $x$; the following equations are derived

$$\frac{d\left(\bar{\varepsilon}^n\right)}{dx} = -\frac{2n}{h_{u,l}\sqrt{3}} \left( \frac{2}{\sqrt{3}} \ln \frac{h_{iu,il}}{h_{u,l}} \right)^{n-1} \frac{dh_{u,l}}{dx} \tag{19}$$

$$\frac{d\left(\dot{\bar{\varepsilon}}^m\right)}{dx} = -\frac{2mV}{Lh_{u,l}\sqrt{3}} \left( \frac{2}{\sqrt{3}} \ln \frac{h_{iu,il}}{h_{u,l}} \right)^{m-1} \frac{dh_{u,l}}{dx} \tag{20}$$

According to Eqs. (15) and (18), the $Q$ parameter is presented to identify for condition before critical strain (strain hardening) and after the critical strain (recovery and softening) as the following formulizations

$$Q_{u,l_{\left(\bar{\varepsilon} \le \varepsilon_C\right)}} = F\left(1 \left[ -\frac{2n}{h_{u,l}\sqrt{3}} \left( \frac{2}{\sqrt{3}} \ln \frac{h_{iu,il}}{h_{u,l}} \right)^{n-1} \right] \dot{\bar{\varepsilon}}^m + \left[ -\frac{2mV_{u,l}}{Lh_{u,l}\sqrt{3}} \left( \frac{2}{\sqrt{3}} \ln \frac{h_{iu,il}}{h_{u,l}} \right)^{m-1} \right] \bar{\varepsilon}^n \right) \exp\left[ C\left( \frac{1}{T} - \frac{1}{T_0} \right) \right] \tag{21}$$

$$Q_{u,l_{\left(\bar{\varepsilon} > \varepsilon_C\right)}} = \left( \left[ F_2 \left( 2a\left( \bar{\varepsilon} - \varepsilon_{\max} \right) \right) \exp \left[ a\left( \bar{\varepsilon} - \varepsilon_{\max} \right)^2 \right] \frac{-2}{h_{u,l}\sqrt{3}} \ln \frac{h_{iu,il}}{h_{u,l}} \right] \dot{\bar{\varepsilon}}^m + \left[ -\frac{2mV_{u,l}}{Lh_{u,l}\sqrt{3}} \left( \frac{2}{\sqrt{3}} \ln \frac{h_{iu,il}}{h_{u,l}} \right)^{m-1} \right] \left( F_2 \exp\left[ a\left( \bar{\varepsilon} - \varepsilon_{\max} \right)^2 \right] + F_3 \right) \right) \exp\left[ C\left( \frac{1}{T} - \frac{1}{T_0} \right) \right] \tag{22}$$

Whereas $\bar{\varepsilon}$ and $\dot{\bar{\varepsilon}}$ are the functions of $h_{u,l}$ (Eq. (16) and $h_{u,l}$ is a function of $x$ (Eqs. (2) and (3)), differentiating the constitutive equation of flow stress (Eq. (15)) with respect to $x$ leads to extract a coefficient named $Q_{u,l}$ that corresponds with $\frac{dh_{u,l}}{dx}$. By differentiating of Eqs. (13) and (14) with respect to $x$

$$\frac{d\sigma_u}{dx} = \frac{dp_u}{dx} - 2\sqrt{1-m_u^2} \frac{Q_u}{\sqrt{3}} \frac{dh_u}{dx} \tag{23}$$

$$\frac{d\sigma_l}{dx} = \frac{dp_l}{dx} - 2\sqrt{1-m_l^2} \frac{Q_l}{\sqrt{3}} \frac{dh_l}{dx} \tag{24}$$

So, by substituting Eqs. (23) and (24) into relations (8) and (9), the following terms are defined

$$A = \left( \frac{d\sigma_u}{dx} + \frac{d\sigma_l}{dx} \right) = \frac{dp_u}{dx} + \frac{dp_l}{dx} - \frac{2}{\sqrt{3}} \left( \sqrt{1-m_u^2}\, Q_u \frac{dh_u}{dx} + \sqrt{1-m_u^2}\, Q_l \frac{dh_l}{dx} \right) \tag{25}$$

$$B = \left( \frac{d\sigma_l}{dx} - \frac{d\sigma_u}{dx} \right) = \frac{dp_l}{dx} - \frac{dp_u}{dx} + \frac{2}{\sqrt{3}} \left( \sqrt{1-m_u^2}\, Q_u \frac{dh_u}{dx} - \sqrt{1-m_l^2}\, Q_l \frac{dh_l}{dx} \right) \tag{26}$$

Therefore, the below equations can be obtained

$$\frac{dp_u}{dx} = \frac{A-B}{2} + \frac{2}{\sqrt{3}} \left( \sqrt{1-m_u^2}\, Q_u \frac{x}{\sqrt{{R_u}^2 - x^2}} \right) \tag{27}$$

$$\frac{dp_l}{dx} = \frac{A+B}{2} + \frac{2}{\sqrt{3}}\left(\sqrt{1-m_l^2}\, Q_l \frac{x}{\sqrt{R_l{}^2-x^2}}\right) \tag{28}$$

$$\frac{d\tau}{dx} = -\frac{2x}{hR_{eq}}\tau - \frac{(p_l - p_u)}{h} - \left(\frac{\tau_l}{R_l} - \frac{\tau_u}{R_u}\right)\frac{x}{h} \tag{29}$$

In this step of the calculations, aimed to function ODE45 as MATLAB's standard solver for ordinary differential equations (ODEs), the above ordinary differential equations are solved. The mentioned function executes a Runge–Kutta method with a variable time step for effective estimation. Hence, the unknown terms of $p_u$ and $p_l$ can be obtained for triple zones of the roll gap.

For determination of unknown terms of equilibrium equations of triple zones, the neutral point position in the roll gap length and boundary conditions for each zone separately needs to be defined. Therefore, due to the material volume constancy principal of the roll gap, the neutral point location is determined based on the following equation [6, 10, 21]:

$$x_{nu} = \sqrt{V_A x_{nl}^2 + (V_A - 1)\frac{h_0}{R_A}} \tag{30}$$

where $V_u$, $V_l$, and $V_A = V_l/V_u$ are the circumferential speed of rolls and speed rate, respectively. $R_{eq} = 1/R_{eq} - h_o/2R_{eq}^2$ is the equivalent roll radius. In addition, $x_{nu}$ and $x_{nl}$ are the horizontal locations of the upper and lower neutral points, respectively.

Because there is no force imposing on the end face of the outlet portion of the slab, the boundary condition of the third zone is known, consequently. Since the deformed region continuity can be used for the determination of the position of neutral points, the boundary conditions of the overall deformed region can be defined, as a result. In the inlet portion of the slab, there is no free-stress condition same as in the outlet portion. Therefore, for assuming the horizontal entrée of the slab into the roll gap, the loading force on inlet portion is one of the unknown terms which should be known for solving the related equations of inlet portion. This loading force is calculated based on the continuity principle of the cross-section region and an entrance portion of the roll gap.

In the present model, assuming no forward tension or compression imposing on inlet portion, the imposed axial force will be zero [3]. This technique is applied because it is near to the real condition of the process in reverse mill rolling. So, with a condition of zero values of the axial normal mean stress $(\sigma_u + \sigma_l)/2 = 0$ in the inlet portion and implementing the bi-section method, the position of neutral points is determined easily.

Considering the mentioned boundary conditions, determination of the position of the triple zone is performed by guessing the position of the $x_{nl}$ varying between a position near the entry section and near the exit section along the length of the roll gap. Using the assumed $x_{nl}$, the supposition of $x_{nu}$ can be calculated by Eq. (30). So, the roll gap can be divided into three assumed zones. Now, the governing differential equations (Eqs. (27)–(29)) can be solved for three assumed zones. The next step is the calculation of the normal mean stress for each iterated case. This iteration manner is continued until the guessed $x_{nl}$ and $x_{nu}$ lead to a zero value of the normal mean stress. Thus, the true locations of the neutral points can be found in the case of the corresponding zero mean axial stress.

After the precise positioning of neutral points and analysis of the differential equations of overall points for triple zones of the roll gap, the rolling force in per slab width unit can be calculated as follows [21]

$$F_u = \int_0^l \left(p_u + \frac{x}{R_u}\tau_u\right)dx \tag{31}$$

$$F_l = \int_0^L \left(p_l + \frac{x}{R_l}\tau_l\right)dx \tag{32}$$

$$T_u = \int_0^L \tau_u R_u dx \tag{33}$$

$$T_l = \int_0^L \tau_l R_l dx \tag{34}$$

In the rolling process, the elastic deformation of the rolls' surfaces of the contact interface with the deformed region leads to the roll flattening feature. In order to identify the real conditions of the rolling in the present calculations, the flattened roll radius is calculated using Hitchcock relation.

## 6 Result and discussion

### 6.1 Analytical analysis

The results of the predicted rolling force from the present model were compared with Salimi's model [21] (constant flow stress situation) and Gudur's model [10] (imposing only strain hardening in flow stress), consequently. As shown in Fig. 4a, the pressure distribution on the rolls' surfaces in analytical models is different. In the present model, same as Salimi's model and Gudur's model, the maximum pressure distribution on the rolls' surface is not located into neutral points and there is more than one maximum pick of pressure distribution. In the present model, the property of stress distribution is different because of the imposition of the rate-dependent flow stress.

Position shifting of imposing shear stress at the slab surface leads to abrupt variations of the pressure-distribution gradient. But, stress distributions on the rolls' surfaces in the rolling exit are the same. Because of the presence of bending torque and shear stress, this stress distribution is unequal in CSR and the entrance region of the roll gap. According to Fig. 4b, due to the variation of mean flow stress in the roll gap length, the

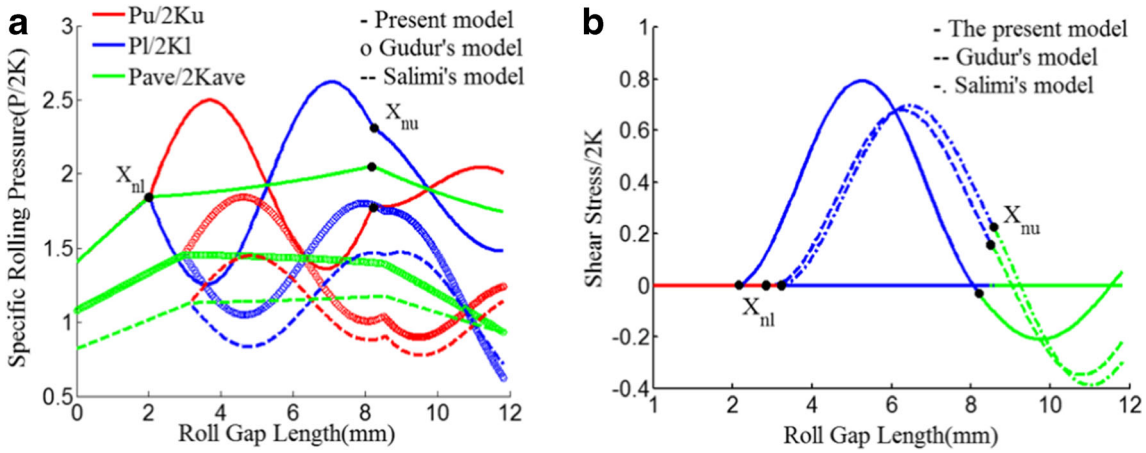


**Fig. 4** Distribution scenario. **a** Pressure distribution. **b** Mean shear stress distribution ($h_i$ = 4.0 mm; $r$ = 10%; $m_u = m_l$ = 0.35; $R_u = R_l$ = 350 mm; VA = 1.05; $K$ = 98.1; $m$ = 0.0542; $n$ = 0.225)

positions of neutral points are moved in the direction of the rolling exit.

Increase of the roll radii leads to the increase of the friction stress and moves the neutral point to the center of the roll gap, consequently. But in the high value of initial thickness, the position of the upper and lower neutral points moves to the entrance and exit of the roll gap. The difference effect of initial thickness on the position of the neutral points is caused by the increase in imposing bending moment onto the deformation region. However, the slab thickness and the roll radii have negligible effect on the position shifting of neutral points.

The comparative positions of neutral points of models under different conditions of thickness reduction are shown in Fig. 5a. As seen in this figure, by increasing the thickness reduction per rolling pass, the location of the neutral points moves to the center of the roll gap and the length of CSR is reduced. On the other hand, increasing the thickness reduction leads to the occurrence of the condition of symmetrical rolling. So it can be concluded that imposing the rate-dependent and strain-hardening conditions in the present model leads to increasing the length of CSR.

The variation of neutral point's position versus rolling temperature is shown in Fig. 5b. By increasing the rolling temperature, the location of neutral points moves to the center of the roll gap and the length of CSR is being reduced as a result.

### 6.2 Experimental verification

In the first section, regarding the material flow formulation of carbon steel considered by Yanagida and Yanagimoto [25], the thermomechanical rolling of pressure vessel steel grade of P265GH was carried out using the wide 4Hi-single stand reversing mill of Khouzestan Oxin Steel Co. (KOSC). This wide rolling mill stand is shown in Fig. 6. Gap control of the rolling passes is performed by signal processing of X-ray thickness gauge. The dimensions of the rolled slab are measured by γ-ray profile meter device of 1-μm accuracy and processing time of 10 ms. The capacity of rolling force is $10^5$ kN.

The rolling force data have been measured by a couple of Kelk disk type load cells with $56 \times 10^3$ kN capacity and

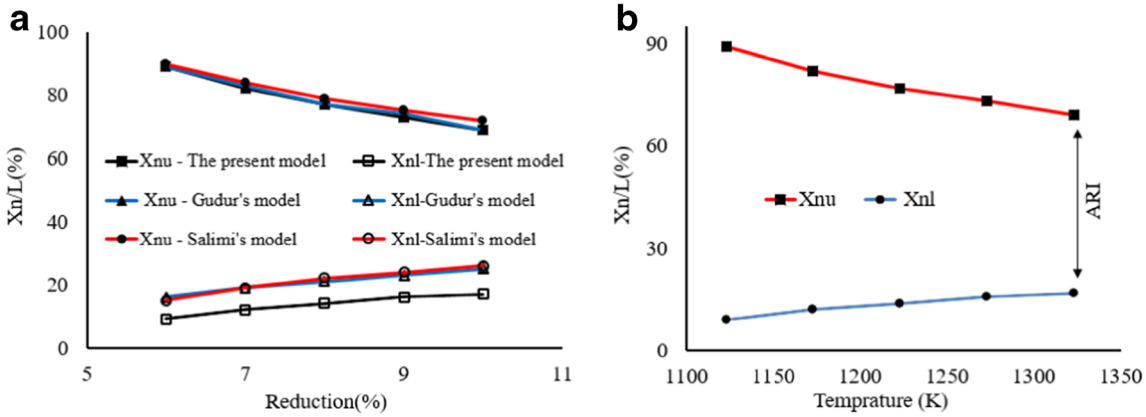


**Fig. 5** Asymmetrical index variations. **a** ARI versus thickness reduction. **b** ARI versus rolling temperature ($h_i$ = 4.0 mm; $m_u = m_l$ = 0.35; $R_u = R_l$ = 350 mm; VA = 1.05; $K$ = 98.1; $m$ = 0.0542; $n$ = 0.225)


**Fig. 6** 4Hi-single stand reversing mill

response time less than 0.1 ms. The broadsiding rolling schedule of a P265GH slab is given in Table 1.

In the second section of experimental work, based on inverse analysis (IA) method introduced by Yanagida et al. [22], the flow behavior of X70 was considered. Then, the verification of the analytical model was verified using rolling schedule setup.

The hot compression tests of X70 were performed under different high temperatures of 850 − 1150 °C and strain rates of $0.001-1\ s^{-1}$ to acquire the constitutive flow model of X70. The evaluation of the experimental results of hot compression tests leads to the extraction of a general form of X70 flow model as follows

$$\begin{cases} \bar{\sigma} = 135.3\bar{\varepsilon}^{0.174}\dot{\bar{\varepsilon}}^{(0.000116T-0.01337)}\exp\left[5225\left(\frac{1}{T}-\frac{1}{1273}\right)\right] & \left(\bar{\varepsilon}\le\varepsilon_c\right) \\ \bar{\sigma} = \left(66\exp\left[-9.6\left(\bar{\varepsilon}-\bar{\varepsilon}_{\max}\right)^2\right]+51.6\right)\dot{\bar{\varepsilon}}^{(0.000116T-0.01337)} & \\ \quad\times\exp\left[5225\left(\frac{1}{T}-\frac{1}{1273}\right)\right] & \left(\bar{\varepsilon}>\varepsilon_c\right) \end{cases} \tag{35}$$

The complete rolling schedule of a X70 slab is given in Table 2. Reference source not found. There are two groups of pass in the schedule named broadsiding and finishing. The broadsiding passes are roughing passes performed to increase the width of the slab and austenite grain refining. The finishing passes are performed under non-recrystallization temperature for obtaining the target thickness of plate and the final fine grain of ferrite structure.

As shown in Fig. 7a, the comparison of calculated outcomes of Salimi's, Gudur's, and the present model with experimental results of thermomechanical rolling signifies a good acquisition of the rolling force with a mean error of 7.6%. As indicated in this figure, the calculated rolling force of the Salimi's model is lower than that of the Gudur's model. Because, in the Salimi's model, the value of yield stress is constant during the rolling process, while the Gudur's model has included the strain hardening effect in the rolled material.

This figure implies that the calculated amounts of the rolling force of the present model are bigger than the measured ones and by an increase of thickness reduction the error extent is being reduced. Referring to Salimi's and Gudur's researches [10, 21], these models have just been investigated in the rolling condition of low initial thickness and thickness reduction range without imposing the condition of rate dependent, work hardening, and softening.

Because of the lack of the mentioned imposing condition in Salimi's and Gudur's model, by increasing the thickness reduction of middle rolling passes, the calculated error of these models is being intensified.

As shown in Fig. 7b, the comparison of calculated outcomes of the present model with experimental results of thermomechanical rolling of X70 microalloy steel signifies a good acquisition of the rolling force with a mean error of 5.06%.

### 6.3 Design of experiments

In the processes parameters study of a set of controllable variable parameters, the design of experiments (DOE) methodology is applied to design an optimum trial layout. As a useful DOE tool, response surface methodology

**Table 1** Thermomechanical rolling schedule of P265GH slab

| Pass no. | Thickness (mm) | Reduction (%) | Width (mm) | Temperature (K) | Rolling speed (mm/s) | Pass type |
|---|---|---|---|---|---|---|
| 1 | 203 | 6.47 | 3488 | 1348 | 2499 | Broadsiding |
| 2 | 189.473 | 6.21 | 3470 | 1338 | 2535 | |
| 3 | 177.705 | 8.63 | 3476 | 1336 | 2517 | |
| 4 | 162.363 | 5.49 | 3470 | 1332 | 2633 | |
| 5 | 153.449 | 9.91 | 3478 | 1329 | 2650 | |
| 6 | 138.245 | 8.67 | 3477 | 1326 | 2705 | |
| Initial dimension of slab (mm): 203 × 1611 × 3478 | | | | | | |

**Table 2** Thermomechanical rolling schedule of X70 slab

| Pass no. | Thickness (mm) | Reduction (%) | Width (mm) | Temperature (K) | Rolling speed (mm/s) | Pass type |
|---|---|---|---|---|---|---|
| 1 | 232 | 5.67 | 4558.99 | 1354.4 | 2.59 | Broadsiding |
| 2 | 219.75 | 6.01 | 4560.09 | 1352.68 | 2.64 | |
| 3 | 206.54 | 6.4 | 4561.27 | 1350.81 | 2.69 | |
| 4 | 193.33 | 6.83 | 4562.53 | 1348.86 | 2.76 | |
| 5 | 180.12 | 7.33 | 4563.89 | 1346.81 | 2.83 | |
| 6 | 166.91 | 7.92 | 4565.36 | 1344.75 | 2.92 | |
| 7 | 153.7 | 8.6 | 4566.96 | 1342.52 | 3.01 | |
| 8 | 140.48 | 9.4 | 4568.72 | 1339.84 | 3.08 | |
| 9 | 127.27 | 12.21 | 3387.23 | 1329.52 | 3.34 | Finishing |
| 10 | 111.74 | 13.9 | 3390.04 | 1325.85 | 3.44 | |
| 11 | 96.2 | 16.15 | 3393.35 | 1322.23 | 3.55 | |
| 12 | 80.66 | 16.31 | 3396.51 | 1142.67 | 3.69 | |
| 13 | 67.51 | 13.46 | 3398.77 | 1142.63 | 3.86 | |
| 14 | 58.42 | 13.48 | 3400.92 | 1140.86 | 4.01 | |
| 15 | 50.55 | 13.51 | 3402.95 | 1138.29 | 4.07 | |
| 16 | 43.72 | 13.54 | 3404.88 | 1134.48 | 4.14 | |
| 17 | 37.8 | 13.58 | 3406.71 | 1129.13 | 4.21 | |
| 18 | 32.66 | 13.63 | 3408.44 | 1122.05 | 4.26 | |
| 19 | 28.21 | 13.68 | 3410.08 | 1114.06 | 4.32 | |
| 20 | 24.35 | 7.85 | 3410.75 | 1103.96 | 4.38 | |
| 21 | 22.44 | 7.6 | 3411.36 | 1092.14 | 4.42 | |

Initial dimension of slab (mm): 232 × 1853 × 4557

(RSM) was utilized for optimization procedure of process parameters [26].

In this study, Box–Behnken matrix is used to dictate a trial layout for an analytical model in 29 runs for the assessment of four parameters such as speed rate, reduction, initial thickness, and roll radii. The mentioned flow model material of X70 microalloy steel is used in analytical runs. These sets of analytical runs are executed for evaluation of effective numerical factors of rolling force and asymmetrical index. The considered asymmetrical rolling index (ARI) in this work is introduced as the following relation

$$\mathrm{ARI} = \frac{Length\ of\ \mathrm{CSR}\ (x_{nu} - x_{nl})}{Contact\ length\ of\ roll\ \mathrm{gap}\ (L)} \times 100 \tag{36}$$

The levels and limits of the independent variables of the Box–Behenken matrix are given in Table 3.

The dictated analytical layout of the Box–Behnken matrix and their factors' levels are introduced in Table 4.

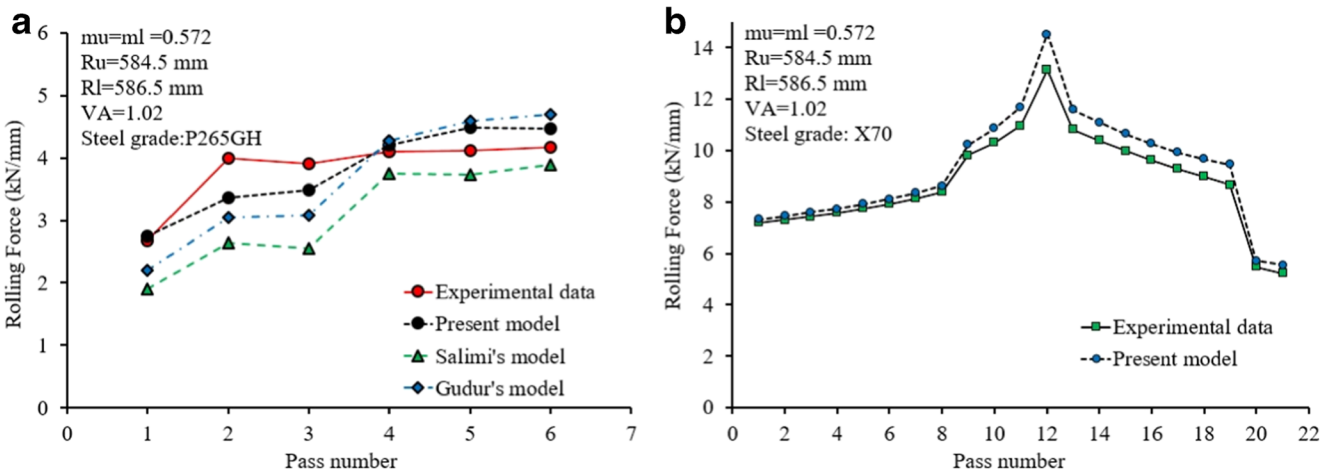


**Fig. 7** Comparison between analytical and experimental results. **a** P265GH. **b** X70

**Table 3** Independent variable levels of the Box–Behenken matrix

| Numerical factors | −1 (low level) | +1 (high level) |
|---|---|---|
| $V_l/V_u$ , speed rate | 1.01 | 1.05 |
| $r$, reduction (%) | 10 | 20 |
| $h_i$ , initial thickness (mm) | 100 | 200 |
| $R$ , roll radii (mm) | 550 | 600 |

### 6.4 ANOVA analysis

The Box–Behnken design technique can evaluate the interaction effects of variable parameters on the response function and estimate a regression model by the implementation of analysis of variance (ANOVA) [26]. The ANOVA is a precise method that, by overall estimation of variance of response function and evaluation of the influence of each parameter on reactions, runs statistical trials to reveal which variables have a major effect on the test runs. When the "$P$ value" is less than 0.05, the factor is taken into account that has a significant effect on the response function with a confidence level of 95% [27].

**Table 4** Analytical layout of the Box–Behnken matrix (material = X70; rolling speed = 2500 mm/s; $m_u = m_l = 0.57$; $R_u = R_l = 586.5$ mm; $T = 1373$ K)

| Run no. | Parameters | | | | Responses (analytical) | |
|---|---|---|---|---|---|---|
| | $V_l/V_u$ | $r$ (%) | $h_i$ (mm) | $R$ (mm) | ARI (%) | Force (kN) |
| 1 | 1.03 | 15 | 150 | 575 | 27.27 | 14.6 |
| 2 | 1.01 | 15 | 150 | 550 | 11.07 | 11.53 |
| 3 | 1.05 | 10 | 150 | 575 | 56.8 | 9.69 |
| 4 | 1.05 | 20 | 150 | 575 | 30.99 | 11.53 |
| 5 | 1.03 | 15 | 150 | 575 | 27.27 | 11.53 |
| 6 | 1.03 | 15 | 100 | 550 | 26.45 | 9.47 |
| 7 | 1.03 | 15 | 150 | 575 | 27.27 | 11.53 |
| 8 | 1.03 | 15 | 150 | 575 | 27.27 | 14.65 |
| 9 | 1.03 | 10 | 200 | 575 | 40.23 | 13.19 |
| 10 | 1.03 | 15 | 150 | 575 | 27.27 | 9.95 |
| 11 | 1.01 | 20 | 150 | 575 | 8.1 | 8.67 |
| 12 | 1.03 | 15 | 200 | 600 | 28.07 | 12.51 |
| 13 | 1.05 | 15 | 100 | 575 | 39.04 | 11.82 |
| 14 | 1.03 | 10 | 150 | 600 | 38.68 | 7.25 |
| 15 | 1.03 | 15 | 200 | 550 | 28.43 | 12.74 |
| 16 | 1.05 | 15 | 150 | 600 | 40.15 | 11.19 |
| 17 | 1.03 | 10 | 100 | 575 | 37.57 | 14.22 |
| 18 | 1.03 | 20 | 100 | 575 | 20.02 | 8.23 |
| 19 | 1.05 | 15 | 150 | 550 | 40.5 | 16.21 |
| 20 | 1.03 | 20 | 150 | 550 | 20.8 | 15.03 |
| 21 | 1.03 | 10 | 150 | 550 | 39.03 | 8.48 |
| 22 | 1.03 | 20 | 200 | 575 | 21.43 | 10.25 |
| 23 | 1.03 | 20 | 150 | 600 | 20.61 | 11.87 |
| 24 | 1.01 | 10 | 150 | 575 | 16.32 | 12.81 |
| 25 | 1.03 | 15 | 100 | 600 | 26.3 | 9.99 |
| 26 | 1.01 | 15 | 150 | 600 | 10.96 | 12.89 |
| 27 | 1.05 | 15 | 200 | 575 | 41.69 | 14.6 |
| 28 | 1.01 | 15 | 100 | 575 | 10.61 | 11.53 |
| 29 | 1.01 | 15 | 200 | 575 | 11.45 | 9.69 |

In this study, ANOVA is used for the identification of the confidence level of the parameter's effect on the ARI. In Table 5, the model summary statistics are given with their regression terms and predicted residual error sum of squares (PRESS). $R^2$, adjusted $R^2$, and predicted $R^2$ are the criteria for the determination of the range of variation of response toward the mean value described by the model; the number of predicted model's terms corresponds to the points in the design matrix and the range of variation for new predicted results, respectively. The definitions of other ANOVA terms are presented in nomenclature. Regarding Table 5, the minimum value of predicted residual error sum of squares (PRESS) and the maximum value of adjusted $R^2$ and predicted $R^2$ is the most suitable model suggested by ANOVA. Hence, this model is selected for analysis of the data [28]. The response surface model of the ARI and rolling force and the contribution effect of parameters on the model's terms are analyzed by ANOVA. The significance of the quadratic model terms is given in Table 6. The model $P$ value less than 0.0001 demonstrates the precise estimation of the models.

For ARI function, the comparison of parameters "$F$ value" and contributions indicated that the speed rate with the highest level of criteria's and the initial thickness with the lowest ones have the major and minor influence on the ARI, respectively [29]. In addition, interaction effects of speed rate–reduction and reduction–roll radii have major and minor effects on the ARI, respectively.

For rolling force function, the comparison of the mentioned criteria indicates that reduction, initial thickness, and interaction of these are the most important parameter influencing the rolling force. Comprising the $F$ value of interaction effect of speed rate–reduction and reduction–initial thickness reveals that the increase of ARI caused to reduce the rolling force.

In thermomechanical rolling process of X70, the mathematical model of the ARI is extracted based on the rolling parameters such as speed rate ($V_l/V_u$), thickness reduction ($r$), initial thickness ($h_i$), and roll radii ($R$). This model can be presented as follows

$$\begin{aligned}\mathrm{ARI} &= f(V_l/V_u, r, h_i, R)\\ &= -5734.5 + 9889.5(V_l/V_u) + 40.5(r) - 0.41(h_i) - 0.07(R)\\ &\quad -43.9(V_l/V_u \times h_i) + 0.45(V_l/V_u \times r) - 0.12(V_l/V_u \times R)\\ &\quad -1.25(r \times h_i) + 0.00032(r \times R) - 0.000042(h_i \times R)\\ &\quad -4114.5(V_l/V_u)^2 + 0.09(r)^2 + 0.000022(h_i)^2\\ &\quad +0.00004(R)^2\end{aligned} \tag{37}$$

**Table 5** Model summary statistics of ARI and rolling force

| Model | Std. dev. | | $R^2$ | | Adjusted $R^2$ | | Predicted $R^2$ | | PRESS | | |
|---|---|---|---|---|---|---|---|---|---|---|---|
| | ARI | Force | ARI | Force | ARI | Force | ARI | Force | ARI | Force | |
| Linear | 2.52 | 0.15 | 0.9601 | 0.9962 | 0.9535 | 0.9955 | 0.9376 | 0.9940 | 239.16 | 0.84 | |
| 2FI | 2.03 | 0.077 | 0.9806 | 0.9992 | 0.9699 | 0.9988 | 0.9361 | 0.9976 | 244.92 | 0.33 | |
| Quadratic | 0.58 | 0.015 | 0.9988 | 1.0000 | 0.9976 | 1.0000 | 0.993 | 0.9999 | 26.84 | 0.019 | Suggested |

The adequacy of the ARI and rolling force models is checked in Table 7.

The high computed coefficient of the regression amount reveals the precision performance of the obtained model. In addition, the favorable values for the adjusted coefficient of regression and adequate precision in high values (value >4) demonstrate the adequacy of the models [29].

### 6.5 3D graphs and interaction effects

The interaction effects of the studied parameters on the ARI and rolling force are evaluated using the following 3D graphs. From Fig. 8, it is clear that ARI reduces with an increase in thickness reduction and rises due to the increase of speed rate [4]. The combination of the low amount of thickness reduction with the high value of speed rate intensifies the rise of the ARI (Fig. 8a). Because in low reduction, the presence of speed rate increases the difference of bending moment in the upper and lower interface of the roll gap. Hence, in higher values of thickness reduction and lower value of speed rate, the amount of the ARI is at the lowest level. Also, the high level of thickness reduction compensates the effects of speed rate when the initial thickness is constant.

Figure 8b shows the interaction effects of initial thickness and speed rate on the ARI. Regarding this figure and based on the presented ANOVA model terms given in Table 6, the term of initial thickness has the lowest effect on the ARI model and high values of the ARI occurred in high levels of speed rate. From Fig. 8c, e, f, it is found that the parameter of roll radii, initial thickness, and their interaction have minimum effect on ARI.

Figure 8d shows the interaction effects of initial thickness and reduction on the ARI. In constant speed rate with an increase of the levels of reduction, the ARI range is raised. But the variation of initial thickness has a negligible effect on the ARI. In the high level of reduction, reduction of the

**Table 6** ANOVA for quadratic model of the ARI and rolling force

| Source | Sum of squares | | D.F. | Mean square | | *F* value | | *P* value | | Contribution (%) | |
|---|---|---|---|---|---|---|---|---|---|---|---|
| | ARI | Force | | ARI | Force | ARI | Force | ARI | Force | ARI | Force |
| Model | 3827.26 | 140.04 | 14 | 273.38 | 10.00 | 821.29 | 42,979.83 | <0.0001 | <0.0001 | – | – |
| *A*—$V_l/V_u$ | 2719.84 | 9.6E−3 | 1 | 2719.84 | 9.6E−3 | 8171.05 | 41.39 | <0.0001 | <0.0001 | 71.06 | 6E−3 |
| *B*—*r* (%) | 948.39 | 113.65 | 1 | 948.39 | 113.65 | 2849.18 | 4.88E+5 | <0.0001 | <0.0001 | 24.77 | 81.15 |
| *C*—$h_i$ (mm) | 10.66 | 24.68 | 1 | 10.66 | 24.68 | 32.02 | 1.06E+5 | <0.0001 | <0.0001 | 0.27 | 17.62 |
| *D*—*R* (mm) | 0.19 | 1.17 | 1 | 0.19 | 1.17 | 0.57 | 5008.35 | 0.4625 | <0.0001 | 4E−3 | 0.83 |
| *AB* | 77.35 | 2.5E−5 | 1 | 77.35 | 2.5E−5 | 232.38 | 0.11 | <0.0001 | 0.7480 | 2.02 | 2.5E−5 |
| *AC* | 0.82 | 4.0E−4 | 1 | 0.82 | 4.0E−4 | 2.46 | 1.72 | 0.1391 | 0.2110 | 0.02 | 4E−4 |
| *AD* | 0.014 | 2.5E−5 | 1 | 0.014 | 2.5E−5 | 0.043 | 0.11 | 0.8382 | 0.7480 | 3E−4 | 2.5E−5 |
| *BC* | 0.39 | 0.39 | 1 | 0.39 | 0.39 | 1.17 | 1678.39 | 0.297 | <0.0001 | 0.01 | 0.27 |
| *BD* | 6.4E−3 | 0.034 | 1 | 6.40E−3 | 0.034 | 0.019 | 147.05 | 0.8917 | <0.0001 | 1E−4 | 0.024 |
| *CD* | 0.011 | 3.6E−3 | 1 | 0.011 | 3.6E−3 | 0.033 | 15.47 | 0.8582 | 0.0015 | 2E−4 | 0.002 |
| $A^2$ | 17.57 | 4.5E−6 | 1 | 17.57 | 4.5E−6 | 52.79 | 0.019 | <0.0001 | 0.8913 | 0.45 | 3E−6 |
| $B^2$ | 39.47 | 3.2E−4 | 1 | 39.47 | 3.2E−4 | 118.57 | 1.40 | <0.0001 | 0.2567 | 1.03 | 2.3E−4 |
| $C^2$ | 0.02 | 0.094 | 1 | 0.02 | 0.094 | 0.06 | 404.12 | 0.8103 | <0.0001 | 5E−4 | 6.7E−2 |
| $D^2$ | 4.1E−03 | 4.5E−6 | 1 | 4.1E−3 | 4.5E−6 | 0.013 | 0.019 | 0.9123 | 0.8913 | 1E−4 | 3E−6 |
| Residual | 4.66 | 3.2E−3 | 14 | 0.33 | 2.3E−4 | | | | | | |
| Pure error | 0 | 0 | 4 | 0 | 0 | | | | | | |
| Cor. total | 3831.92 | 140.05 | 28 | | | | | | | 100 | 100 |

**Table 7** The adequacy of the ARI and rolling force modelTerms

| Value | | Terms | Value | | |
|---|---|---|---|---|---|
| ARI | Force | | ARI | Force | |
| Std. dev. | 0.58 | 0.015 | $R^2$ | 0.9988 | 1.0000 |
| Mean | 27.64 | 11.48 | Adjusted $R^2$ | 0.9976 | 1.0000 |
| C.V. (%) | 2.09 | 0.13 | Predicted $R^2$ | 0.9930 | 0.9999 |
| PRESS | 26.84 | 0.019 | Adequate precision | 115.416 | 822.407 |

imposed moment on the vertical side of the deformation zone leads to the decrease of the length of CSR and ARI, consequently. The speed rate has a considerable effect on the ARI, generally. Also, this parameter performs an intensifier for the ARI in the rolling process.

As indicated in Fig. 9a–c, increasing the parameters of reduction, initial thickness, and roll radii leads to the increase of the pressure distribution, bending moment onto the vertical side of the roll gap and friction stress, respectively. Hence, the

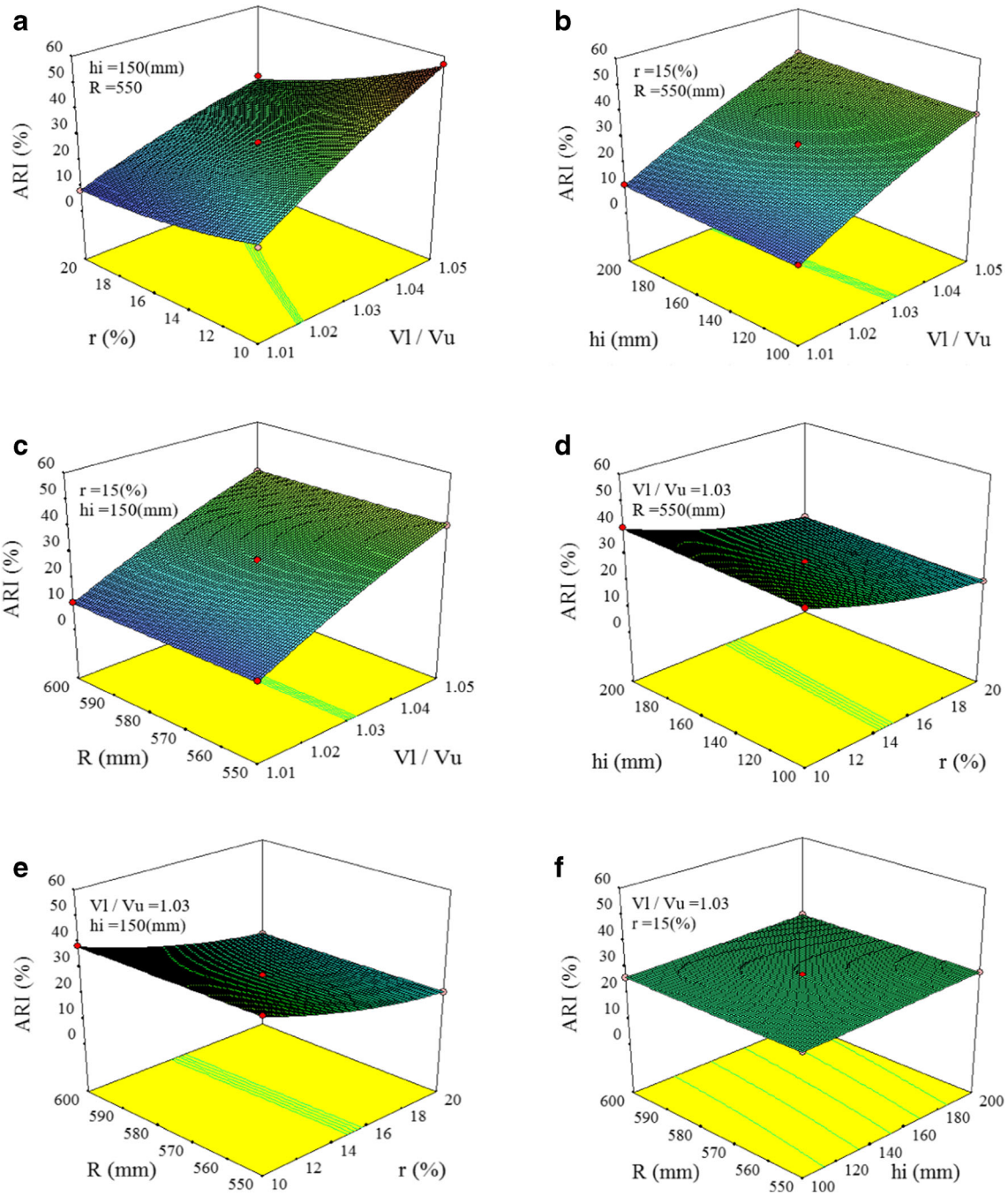


**Fig. 8** The interaction effects of parameters on the ARI. **a** Reduction versus speed rate. **b** Initial thickness versus speed rate. **c** Roll radius versus speed rate. **d** Initial thickness versus reduction. **e** Roll radius versus reduction. **f** Roll radius versus initial thickness

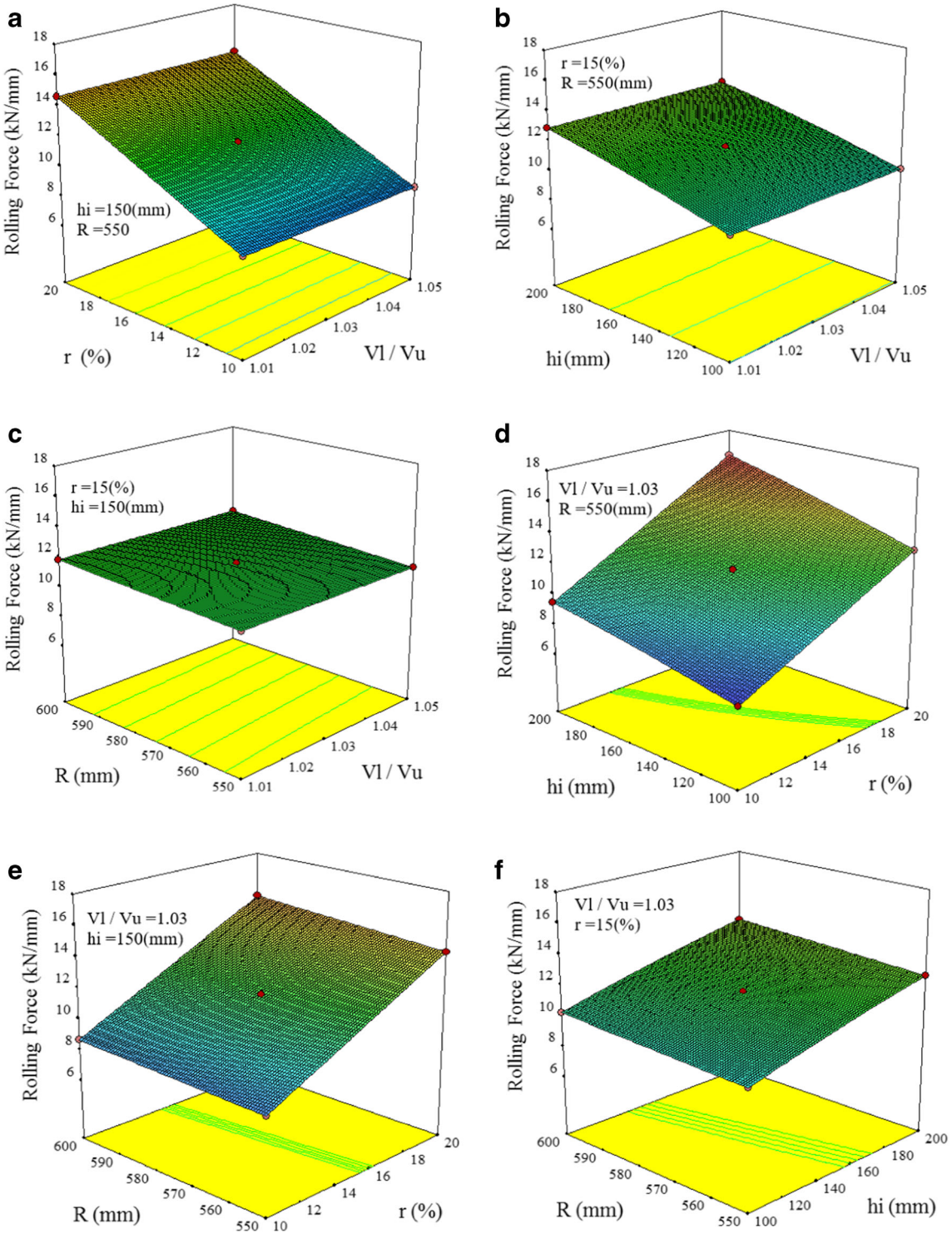


**Fig. 9** The interaction effects of parameters on the rolling force. **a** Reduction versus speed rate. **b** Initial thickness versus speed rate. **c** Roll radius versus speed rate. **d** Initial thickness versus reduction. **e** Roll radius versus reduction. **f** Roll radius versus initial thickness

rolling force value rises, whereas in this range of parameters, the roll radii has negligible effect on the rolling force (Fig. 8c–f).

Furthermore, speed rate and its interaction with roll radii have an unnoticeable effect on the rolling force (Fig. 9c). As the speed rate and the roll radii have a reverse effect on ARI (Fig. 8c), the interaction of these neutralizes their effects on the rolling force. A considerable feature is shown in Fig. 9d where the interaction of thickness reduction and initial thickness increases the value of rolling force, intensively. The cause

of this overlapping is the simultaneous growth of shear stress and imposed moment on vertical sides of the deformed region. Also, as indicated in Fig. 9e, the interaction effect of roll radii and thickness reduction leads to intensification of the imposed friction stress onto vertical side of roll gap and increases the rolling force, consequently.

## 7 Conclusions

In this work, based on the slab analysis method and RSM's design, an advanced analytical model for the calculation of TMR force is presented. In the present model, in addition to imposing visco-plastic flow stress of the rolled material (X70 and P265GH steel grades), the effects of rate-dependent and strain-hardening condition on yield shear stress of the upper and lower surfaces of the rolled slab are investigated. A new index of asymmetry (ARI) is introduced for the rolling process. In the comparison scenario, the ranges of the calculated results of the rolling force in the present model are higher than other models and have a good agreement with experimental data. The outcome results of the presented model are implied in the following concepts:

1. By imposing the strain-hardening condition, the positions of neutral points are moved in the rolling exit direction.
2. Increasing of the rolling temperature and thickness reduction per rolling pass reduces the dimension of the ARI and leads to a reduction of the asymmetrical rolling intensity.
3. The initial thickness has a minimum effect on the ARI level and the speed rate roles as an intensifier of parameters' effect on the ARI.
4. The interaction of thickness reduction and initial thickness increases the value of rolling force. The combination of the high value of speed rate with the low percent of thickness reduction leads to the restricted rise of the ARI level.

## 8 Nomenclature

$a_u$, $a_l$, material constant of the upper and lower surface of slab, respectively; $C$, temperature sensitivity of slab; ***Core. total***, the contrast sum of squared of the single examination versus the comprehensive average. ***C.V.***, coefficient of variation; $D$, work roll material constant; ***degrees of freedom (D.F.)***, the number of separate attainable collations for estimation a parameter; $F$, rolling force per width unit; $F_1$, $F_2$, $F_3$, $n$, slab material constant; $F_{2_u}$, $F_{2_l}$, material constant of the upper and lower surface of slab, respectively; $F_u$, $F_l$, material constant of the upper and lower surface of slab, respectively; $h$, variable slab thickness; $h_i$, $h_o$, slab thickness in entrance and exit of roll gap, respectively; $h_{iu}$, $h_{il}$, upper and lower slab thickness in entrance and exit of roll gap, respectively; $h_u$, $h_l$, upper and lower variable slab thickness, respectively; $k$, mean yield shear stress of the slab; $k_u$, $k_l$, upper and lower mean yield shear stress of the slab, respectively; $L$, contact length of roll gap; ***mean square***, the sum of squares divided to the degrees of freedom parallel to variance; ***model sum of squares***, total of the sum of squares for the all of model terms; ***model D.F.***, generally equal to the sum of model terms minus 1; ***model F value***, a trial for comparison of model versus residual variance; $m$, strain rate dependent parameter of slab; $m_u$, $m_l$, upper and lower friction factor, respectively; $Q_u$, $Q_l$, upper and lower differential stress factor, respectively; ***PRESS***, predicted residual error sum of squares; $p_u$, $p_l$, upper and lower rolling pressure, respectively; ***residual sum of squares***, the total of the sum of squares of the model terms not counting the model; ***residual D.F.***, adjusted total degree of freedom minus the model one; ***RSM***, response surface methodology; $R^2$, coefficient of determination; $R_{eq}$, equivalent roll radius; $R_u$, $R_l$, upper and lower roll radius, respectively; $r$, thickness reduction; ***Std. dev.***, standard deviation; $T$, slab temperature; $T_0$, reference temperature; $T_u$, $T_l$, upper and lower surface temperature of slab, respectively; $V_A$, speed rate of rolls; $V_u$, $V_l$, circumferential speed of the upper and lower roll, respectively; $x$, distance of rolled element from exit of roll gap; $x_{nu}$, $x_{nl}$, distance of the upper and lower rolled element from the exit of roll gap, respectively; $\overline{\varepsilon}_{c_u}$, $\overline{\varepsilon}_{c_l}$, critical equivalent strain of the upper and lower surface of slab, respectively; $\overline{\varepsilon}_{max_u}$, $\overline{\varepsilon}_{max_l}$, maximum equivalent strain of the upper and lower surface of slab, respectively; $\overline{\varepsilon}_u$, $\overline{\varepsilon}_l$, equivalent strain of the upper and lower surface of slab, respectively; $\dot{\overline{\varepsilon}}_u$, $\dot{\overline{\varepsilon}}_l$, equivalent strain rate of the upper and lower surface of slab, respectively; $\mu_u$, $\mu_l$, upper and lower friction coefficient, respectively; $\sigma$, stress at any element of the vertical side of roll gap; $\sigma_u$, $\sigma_l$, stress at any upper and lower element of vertical side of roll gap, respectively; $\sigma_x$, $\sigma_y$, $\tau_{xy}$, normal and shear stresses at any element of roll gap, respectively; $\tau$, mean shear stress at any element of the vertical side of roll gap; $\tau_u$, $\tau_l$, shear stress at the upper and lower surface of roll gap, respectively; $\Delta h$, rolling draft

**Acknowledgements** This work was supported by the Khouzestan Oxin Steel Co. (KOSC). The authors sincerely appreciate the continuous cooperation and encouragement of R&D management.

## References

1. Aboutorabi A, Assempour A, Afrasiab H (2016) Analytical approach for calculating the sheet output curvature in asymmetrical rolling: in the case of roll axis displacement as a new asymmetry factor. Int J Mech Sci 105:11–22
2. Kadkhodaei M, Salimi M, Poursina M (2007) Analysis of asymmetrical sheet rolling by a genetic algorithm. Int J Mech Sci 49(5): 622–634

3. Qwamizadeh M, Kadkhodaei M, Salimi M (2012) Asymmetrical sheet rolling analysis and evaluation of developed curvature. Int J Adv Manuf Technol 61(1–4):227–235
4. Hwang Y-M, Tzou G-Y (1995) An analytical approach to asymmetrical hot-sheet rolling considering the effects of the shear stress and internal moment at the roll gap. J Mater Process Technol 52(2): 399–424. doi:10.1016/0924-0136(94)01731-F
5. Hwang Y, Tzou G (1995) Analysis of asymmetrical hot strip rolling by the slab method. J Mater Eng Perform 4(3):265–274
6. Hwang Y-M, Tzou G-Y (1997) Analytical and experimental study on asymmetrical sheet rolling. Int J Mech Sci 39(3): 289–303
7. Tzou G-Y (1999) Relationship between frictional coefficient and frictional factor in asymmetrical sheet rolling. J Mater Process Technol 86(1):271–277
8. Salimi M, Sassani F (2002) Modified slab analysis of asymmetrical plate rolling. Int J Mech Sci 44(9):1999–2023
9. Mousavi SA, Ebrahimi S, Madoliat R (2007) Three dimensional numerical analyses of asymmetric rolling. J Mater Process Technol 187:725–729
10. Gudur P, Salunkhe M, Dixit U (2008) A theoretical study on the application of asymmetric rolling for the estimation of friction. Int J Mech Sci 50(2):315–327
11. Tian Y, Guo Y-H, Wang Z-D, Wang G-D (2009) Analysis of rolling pressure in asymmetrical rolling process by slab method. J Iron Steel Res Int 16(4):22–38
12. Zhang S, Zhao D, Gao C, Wang G (2012) Analysis of asymmetrical sheet rolling by slab method. Int J Mech Sci 65(1):168–176
13. Chen F, Feng G, Cui Z (2014) Mathematical modeling of critical condition for dynamic recrystallization. Procedia Eng 81:486–491
14. Qwamizadeh M, Kadkhodaei M, Salimi M (2014) Asymmetrical rolling analysis of bonded two-layer sheets and evaluation of outgoing curvature. Int J Adv Manuf Technol 73(1–4):521–533
15. Afrouz F, Parvizi A (2015) An analytical model of asymmetric rolling of unbounded clad sheets with shear effects. J Manuf Process 20, Part 1:162–171. doi:10.1016/j.jmapro.2015.08.007
16. Tang D, Liu X, Song M, Yu H (2014) Experimental and theoretical study on minimum achievable foil thickness during asymmetric rolling. PLoS One 9(9):e106637
17. Byon S, Kim S, Lee Y (2004) Predictions of roll force under heavy-reduction hot rolling using a large-deformation constitutive model. Proc Inst Mech Eng B J Eng Manuf 218(5):483–494
18. Liu J, Kawalla R (2012) Influence of asymmetric hot rolling on microstructure and rolling force with austenitic steel. Trans Nonferrous Metals Soc China 22, Supplement 2:s504–s511. doi: 10.1016/S1003-6326(12)61753-1
19. Wronski M, Wierzbanowski K, Bacroix B, Lipinski P (2015) Asymmetric rolling textures of aluminium studied with crystalline model implemented into FEM. Materials Science and Engineering Conference Series 82(1): xxxxxx
20. Yu HL, Lu C, Tieu AK, Li HJ, Godbole A, Zhang SH (2016) Special rolling techniques for improvement of mechanical properties of ultrafine-grained metal sheets: a review. Adv Eng Mater 18(5):754–769
21. Salimi M, Kadkhodaei M (2004) Slab analysis of asymmetrical sheet rolling. J Mater Process Technol 150(3):215–222
22. Yanagida A, Liu J, Yanagimoto J (2003) Flow curve determination for metal under dynamic recrystallization using inverse analysis. Mater Trans 44(11):2303–2310
23. Galantucci LM, Tricarico L (1999) Thermo-mechanical simulation of a rolling process with an FEM approach. J Mater Process Technol 92–93:494–501. doi:10.1016/S0924-0136(99)00242-3
24. Siciliano F Jr, Jonas JJ (2000) Mathematical modeling of the hot strip rolling of microalloyed Nb, multiply-alloyed Cr-Mo, and plain C-Mn steels. Metall Mater Trans A 31(2):511–530
25. Yanagida A, Yanagimoto J (2005) Regression method of determining generalized description of flow curve of steel under dynamic recrystallization. ISIJ Int 45(6):858–866
26. Box G, Wilson K (1951) On the experimental attainment of optimum condition. J Royal Statistical Soc 13:1–45
27. Ayaz M, Khaki DM, Arab NBM (2014) Influence of hot rolling on formability of Nb-microalloyed steel: an experimental design study. Trans Indian Inst Metals 67(3):429–436
28. Davidson MJ, Balasubramanian K, Tagore G (2008) Surface roughness prediction of flow-formed AA6061 alloy by design of experiments. J Mater Process Technol 202(1):41–46
29. Razani N, Aghchai AJ, Dariani BM (2014) Flow-forming optimization based on hardness of flow-formed AISI321 tube using response surface method. Int J Adv Manuf Technol 70(5–8):1463–1471